CMS Physics Analysis Summary

Contact: cms-pag-conveners-top@cern.ch 2016/03/13

Measurement of the top quark mass from single-top production events

The CMS Collaboration

Abstract

We measure the mass of the top quark from events where a single top quark is produced. The analysis is performed on data from pp collisions collected by the CMS detector at a center of mass energy of 8 TeV. The top quark is reconstructed from its decay $t \to W^+b$, with the W boson decaying leptonically in the muon channel. Specific event topology and kinematic properties are used in order to enrich the sample in single-top-quark events in the t-channel, at the expense of top-quark pair production events. For the single-top quark component, a fit to the reconstructed top invariant mass distribution yields $m_t = 172.60 \pm 0.77\ (\text{stat})\ ^{+0.97}_{-0.93}\ (\text{syst})$ GeV.

1 Introduction

At the Large Hadron Collider (LHC), top quarks are produced mainly in top anti-top quark pairs, $t\bar{t}$, through gluon-gluon fusion or quark-antiquark annihilation, that proceed via the strong interaction. The Standard Model (SM) predicts sizable single-top quark production through electroweak processes, as was indeed observed [1–3]. Single-top quark production at the lowest order in perturbation theory is characterized by the *t*-channel, *s*-channel and associated tW production processes. Figure 1 shows Feynman diagrams for the t-channel, the dominant process in terms of cross section, about 85 pb at $\sqrt{s} = 8$ TeV [4]. At 8 TeV the cross sections for the single top s-channel and associated tW production are about 5.6 and 22.4 pb, respectively, while the cross section for $t\bar{t}$ production is about 250 pb [4].

Figure 1: Dominant Feynman diagrams for single top quark production in the *t*-channel in leading order five-flavour scheme $2 \to 2$ (left) and next-to-leading order four-flavour scheme $2 \to 3$ (right) processes.

Most measurements of the top quark mass to date are obtained from samples of $t\bar{t}$ events. However, measuring the top quark mass in single-top quark production enriches the range of available measurements, with systematic uncertainties partially uncorrelated from those considered in $t\bar{t}$ production. The different production mechanism at work, that features a very different color flow, is also a useful check that there are no large "unknown" systematic effects in top quark mass measurements due to the modelling of non-perturbative QCD effects.

The current world average of the top quark mass is 173.34 ± 0.76 GeV [5]. A combination of CMS measurements from data at 7 and 8 TeV yields $m_t = 172.44 \pm 0.13\,(\text{stat}) \pm 0.47\,(\text{syst})$ GeV [6]. The ATLAS Collaboration recently reported a measurement of the top quark mass using a sample enriched in single top quark *t*-channel events, obtaining a value of $m_t = 172.2 \pm 0.7\,(\text{stat}) \pm 2.0\,(\text{syst})$ GeV [7].

In this analysis, top quark candidates are reconstructed via their decay to a W boson and a b quark, where the W decays to a muon and a neutrino. The selection is tailored to enhance the single-top quark content in the final sample in order to have a result as independent as possible from those obtained from $t\bar{t}$. A blinded analysis approach has been used: the optimization of the event selection and the choice of the fit technique were finalized before obtaining the final result on the data sample.

2 Datasets

The measurement reported here is performed using the proton-proton collision data sample collected in 2012 at 8 TeV by the CMS detector [8], corresponding to an integrated luminosity of 19.7 fb^{-1}.

Simulated events are used to optimize the event selection, study the backgrounds and the ex-

pected performance. The simulated signal t-channel events are generated with the POWHEG generator, version 1.0 [9], interfaced to PYTHIA 6.4 [10] for parton shower and hadronisation. Other single-top-quark channels, the s-channel and tW associated production, are considered as backgrounds for this measurement and simulated with the same generators. Top quark pair production, single vector-boson production associated with jets (referred to as W/Z+jets in the following), and double vector boson (diboson) production are amongst the backgrounds taken into consideration and have been simulated with the MADGRAPH generator, version 5.148 [11], interfaced to PYTHIA for parton showering. In addition, the PYTHIA generator is also used to simulate QCD multijet samples enriched with isolated muons. The value of the top-quark mass used in all simulated samples is 172.5 GeV. All samples are generated using the CTEQ6.6M [12] PDF set. The factorisation and renormalisation scales are both set to m_t for the single-top-quark samples, while a dynamic scale is used for the other samples. The passage of particles through the detector is simulated using the Geant4 toolkit [13]. The simulation includes additional pileup pp collisions with a multiplicity which matches the one observed in data.

3 Event selection and reconstruction

We use the same event reconstruction and selection of top quark candidates adopted by the CMS single top quark t-channel cross section measurement at 8 TeV [2]. Due to the detector acceptance and jet selection requirements, signal events are characterized by the presence of two reconstructed jets, one of which comes from the hadronization of a b quark. Therefore events with two reconstructed jets, out of which one is b-tagged, constitute our "signal sample" (referred to as '2J1T' in the following). Other event topologies are useful to study background properties: the sample with two reconstructed jets, none of which is b-tagged ('2J0T') is dominated by W+ jets events; the sample with three reconstructed jets, where two jets are b-tagged ('3J2T') is dominated by $\mathrm{t\bar{t}}$ + jets events.

Events are selected online by the high-level trigger system by asking for the presence of one isolated muon candidate with transverse momentum (p_T) greater than 24 GeV and absolute value of the pseudorapidity (η) below 2.1. Events are required to have at least one primary vertex reconstructed from at least four tracks, with a distance from the nominal beam-interaction point of less than 24 cm along the z axis and less than 2 cm in the transverse plane. In cases where more than one primary vertex is found, the one featuring the largest value of Σp_T^2 is retained, where Σp_T^2 is the sum of the squared transverse momenta of all the tracks assigned to that vertex. All particles are reconstructed and identified with the CMS particle flow algorithm [14, 15]. Muon candidates for analysis are further required to have $p_T > 26$ GeV. This requirement ensures that the selected muons are in the plateau region of the trigger turn-on curves. Muon candidates are also required to be isolated. This is ensured by requiring that the variable I_{rel} be below 0.12. Here I_{rel} is defined as the sum of the transverse energies deposited by stable charged hadrons, photons, and neutral hadrons in a cone of size $\Delta R = \sqrt{(\Delta\eta)^2 + (\Delta\phi)^2} = 0.4$, ($\phi$ being the polar angle) corrected by the average contribution of neutral particles from overlapping pp interactions (pileup), and divided by the muon p_T itself. Events are rejected if an additional muon candidate is present. For this purpose, a looser selection is required for additional muons: $p_T > 10$ GeV, $|\eta| < 2.5$, and $I_{\mathrm{rel}} < 0.2$.

To define jets, we cluster the reconstructed particles with the anti-k_{T} algorithm [16] using a distance parameter of 0.5. In the algorithm, charged particles are excluded if they are closer to any primary vertex (along the z axis) than they are to the leading vertex. The average energy density of neutral particles that are not clustered into jets is used to estimate the energy due to pileup interactions in the jet cone, and a corresponding correction to the jet energy is de-

rived. Additional corrections to the jet energies are derived from the study of dijet events and photon+jets events [17]. Jets are required to have $\eta < 4.5$ and to have a calibrated transverse energy greater than 40 GeV. Jets coming from b quarks are identified using a b-tagging algorithm based on the the 3D impact parameter of the tracks in the jet to define a b-discriminator [18]. We apply a selection on this discriminator variable such that the probability to misidentify jets coming from the hadronization of light quarks (u, d, s) or gluons is small (0.1%) while retaining an efficiency of selecting jets coming from b quarks at 46%, as determined from simulation of events with top-quark topologies.

The missing transverse energy ($E_{\mathrm{T}}^{\mathrm{miss}}$) is calculated as the magnitude of the negative vector sum of the transverse momenta of all reconstructed particles. We require this quantity to exceed 50 GeV, in order to suppress QCD multijet background.

In addition, we apply a cut on the root-mean-square $\eta - \phi$ radius of the particles with respect to the axis of non b-tagged jets, $\mathrm{RMS}(\Delta R) < 0.025$, in order to reject jets from pileup, and a cut on the transverse mass of the W boson, $m_{\mathrm{T}}(\mathrm{W}) > 50\,\mathrm{GeV}$, in order to further suppress background from multijet QCD events, where $m_{\mathrm{T}}(\mathrm{W}) = \sqrt{\left(p_T^{\mu} + E_{\mathrm{T}}^{\mathrm{miss}}\right)^2 - \left(p_x^{\mu} + p_{\mathrm{T},x}^{\mathrm{miss}}\right)^2 - \left(p_y^{\mu} + p_{\mathrm{T},y}^{\mathrm{miss}}\right)^2}$, where $E_{\mathrm{T}}^{\mathrm{miss}}$, $p_{\mathrm{T},x}^{\mathrm{miss}}$ and $p_{\mathrm{T},y}^{\mathrm{miss}}$ are the missing energy and the components of the missing momentum in the plane transverse to the beam axis.

In order to enrich the sample in single-top quark events, further cuts are applied to variables which exhibit good discriminating power with respect to $\mathrm{t\bar{t}}$ events, as described below.

A feature of single-top quark production in the t channel is that the top quark is accompanied by a light jet in a relatively forward direction with respect to $\mathrm{t\bar{t}}$ and other background processes (the quark labelled q' in Fig. 1). This is reflected in the distribution of the absolute value of the pseudo-rapidity of the light jet $|\eta_{\mathrm{j}'}|$, shown in Fig. 2, left. A cut at $|\eta_{\mathrm{j}'}| > 2.5$ is applied to the sample.

While for $\mathrm{t\bar{t}}$ production an equal amount of top and anti-top quarks is produced, in the case of t-channel single top quark production, top quarks are produced more abundantly than anti-top quarks, due to the charge asymmetry of the proton-proton initial state [4]. Only events with positively charged muons are retained for the mass measurement. Fig. 2, right, shows the distribution of the reconstructed top charge.

4 Determination of the mass

Using the algorithm described in [19], a top quark candidate is reconstructed from the muon, $E_{\mathrm{T}}^{\mathrm{miss}}$, and b-jet; and its mass, $m_{\ell\nu b}$, is derived. The 4-momenta of the muon and the jet are measured, while, for the neutrino, the 4-momentum is determined by using the missing transverse energy in the event, and the contrstrain that the muon and the neutrino come from a W boson decay. Fig. 3 shows the reconstructed top mass distribution before and after this final selection: the level of agreement between data and simulation is very good. The fraction of reconstructed top quarks from single-top quark production is about 75% of the surviving top quark sample (about 71% from t-channel production).

The top-quark mass is measured with an extended unbinned maximum likelihood fit to the reconstructed invariant mass $m_{\ell\nu b}$. The number of events for the various contributions, except for the single-top quark t-channel, is fixed to values obtained from the single top quark t-channel cross section measurement [2]. The description of the parametrization of the signal and background components used in the fit is presented below. The free parameters of the fit

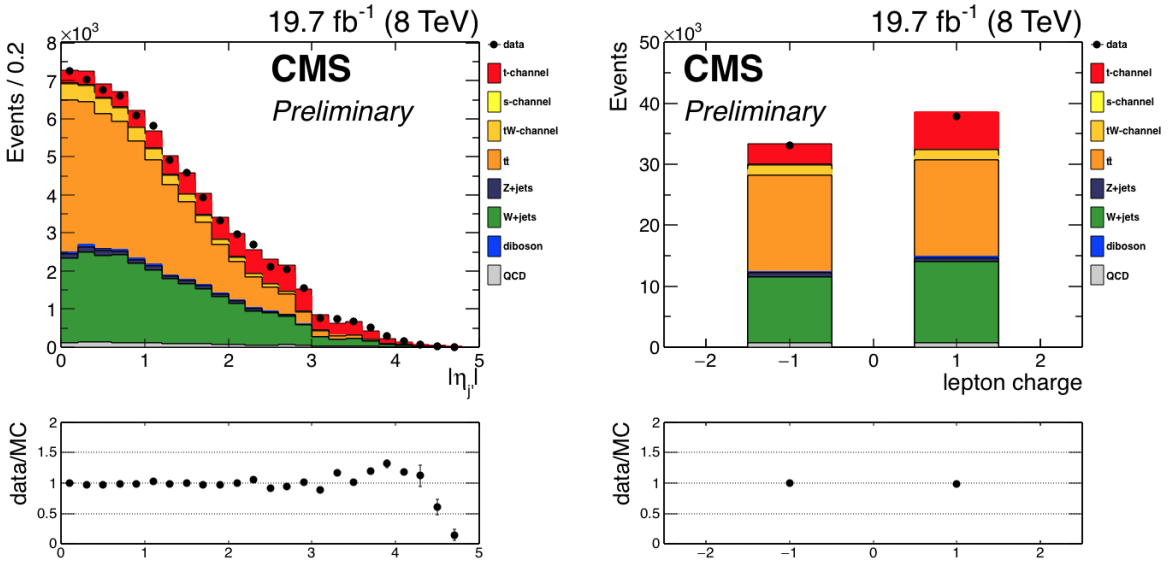

Figure 2: Distribution of the light jet pseudorapidity (left) and of the reconstructed top quark charge (right). Points represent real data, stacked histograms show expected contributions from different event classes in simulated data. Bottom plots show the ratio of the observed number of events in real data to the number predicted by simulation.

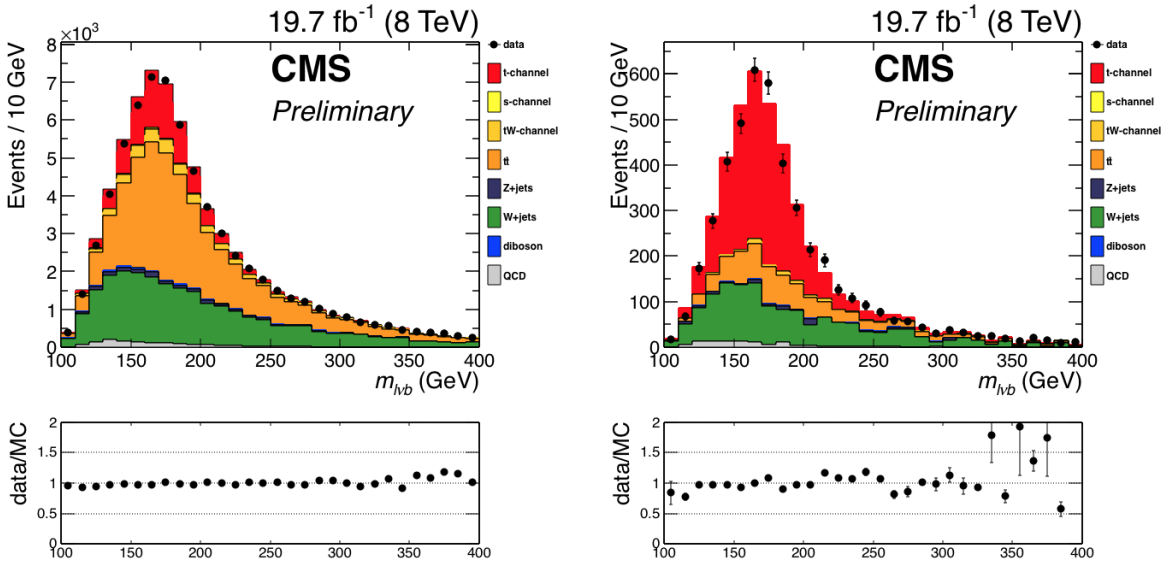

Figure 3: Reconstructed top quark mass distribution for data (points) and Monte Carlo events (stacked histograms). Top: initial selection; bottom: final selection after charge and light jet pseudorapidity cuts. Bottom plots show the ratio of the observed number of events in real data to the number predicted by simulation.

are the number of single-top-quark signal events and the parameters of the signal shape, as described in the following.

4.1 Signal parametrization

We study the signal shape on simulation. The signal includes all channels where a top quark is produced. After the full selection, the sample mostly consists of a single top quark t-channel and a $\mathrm{t\bar{t}}$ component.

The invariant mass distributions of these two samples cannot be satisfactorily described by a unique shape. In fact the $\mathrm{t\bar{t}}$ component exhibits a wider peak, with a larger high-mass tail, as expected from studies on the simulation that show that, for $\mathrm{t\bar{t}}$ events, the number of muon-b-jet pairs correctly assigned to the parent top quark is around 55%, while this fraction exceeds 90% for simulated signal events. Both contributions can however be fit by Crystal Ball distributions [20] with independent parameters. The distributions obtained from the full simulated samples before the final selection are shown in Fig. 4. The fitted values of the mass (muCB parameter of the Crystal Ball function) differ by about 2σ: $m_{\mathrm{t}}(t\text{-channel}) - m_{\mathrm{t}}(\mathrm{t\bar{t}}) = 0.38 \pm 0.17\,\mathrm{GeV}$.

The remaining single-top quark components (s-channel and tW production) only account for about 3.5% in the final sample and their contribution is absorbed in the $\mathrm{t\bar{t}}$ component, since the distributions exhibit broader peaks with respect to the t-channel.

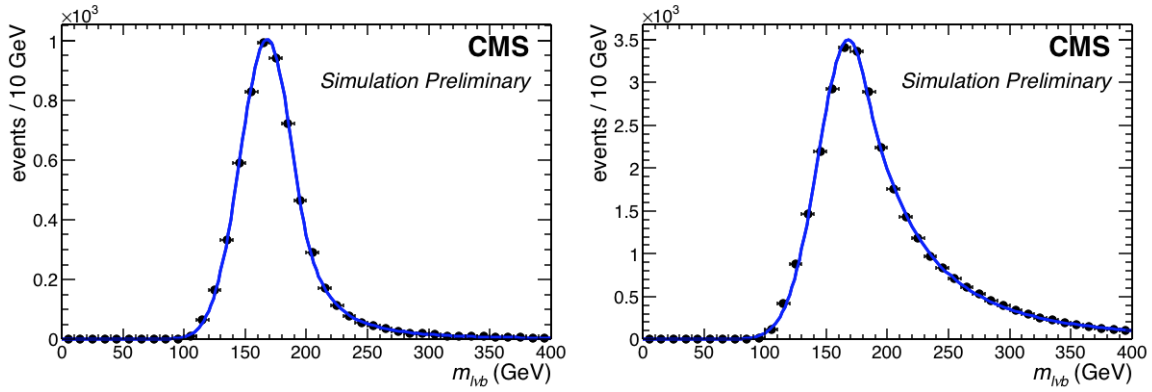

Figure 4: Signal shape from Monte Carlo simulation. Left: single top t-channel events; right: $\mathrm{t\bar{t}}$ events. The continuous blue lines show the results of fits to Crystal Ball shapes.

Since the simulated samples are generated with a top-quark mass value of $m_{\mathrm{t}}(\mathrm{gen}) = 172.5\,\mathrm{GeV}$, the fit might return shifted values. In order to correct for a possible shift and understand the dependence of the shift from the actual value of the mass, we performed the mass fit on a set of simulated samples: for each of them, the t-channel single-top quark and the $\mathrm{t\bar{t}}$ subsamples are generated with different values for the top-quark mass; all other subsamples remained unchanged. From the results of these fits, a "calibration curve" relating the observed mass shift to the fitted mass value, is obtained. Fig. 5 shows the resulting values of the fitted top mass as a function of the generated mass (left) and a "mass calibration curve" from a fit to these values (right). The correction to be applied to the fitted value appears as a linear function of the fitted value itself. The shaded grey area represents the systematic uncertainty associated to the correction, derived from the statistical errors of the fits.

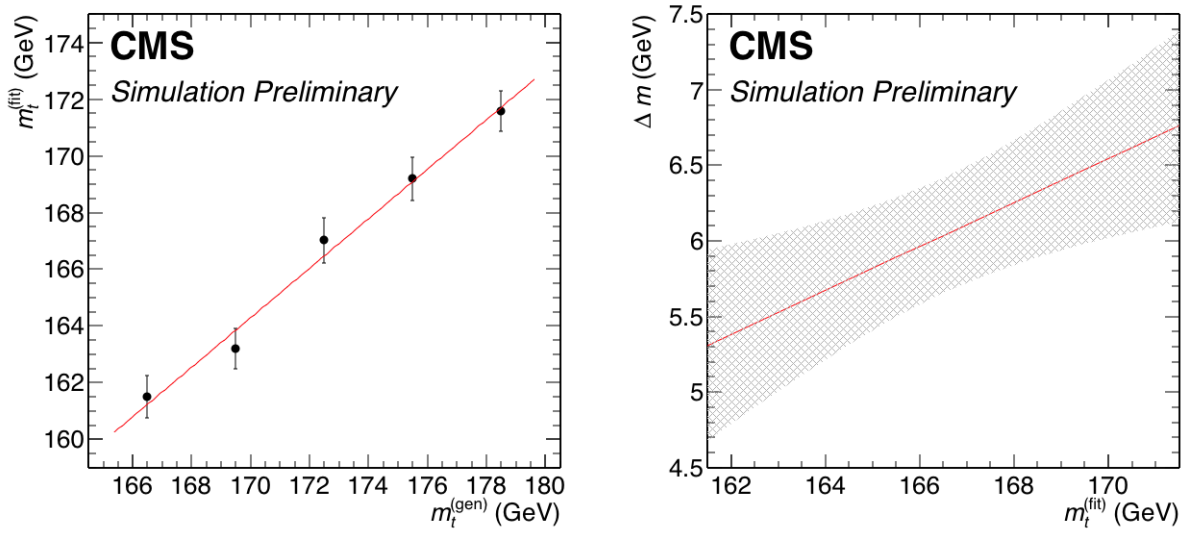

Figure 5: Mass calibration from fits to samples with different generated top mass. Left: fit results as a function of the generated top mass. The red line shows the result of a linear fit to the points. Right: mass correction, as a function of the fitted top mass (red line). The shaded grey area represents the associated systematic uncertainty.

4.2 Background parametrization

The residual background is expected to be dominated by W+jets events. The '2J0T' sample is dominated by such events and has large statistics. Simulations show significant differences in the reconstructed top-quark mass distribution with respect to the '2J1T' sample. The background shape in simulated events is well reproduced by a Novosibirsk function [21]. However, the parameters of the fitted function vary significantly as a function of the cut on $|\eta_{j'}|$ (see Fig. 6). Therefore, the simulated sample is used to determine the shape parameters in the final fit.

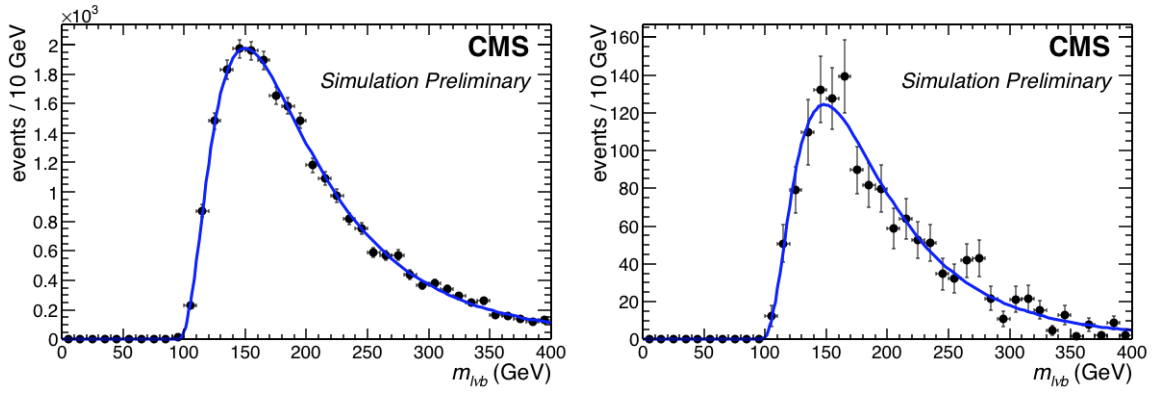

Figure 6: Background shape from Monte Carlo simulation. Left: before final selection; right: after final selection. The continuous blue lines show the results of fits to Novosibirsk functions.

4.3 Determination of the top quark mass from the fit

The invariant mass distribution of the selected top quark candidates is fit to the sum of a single-top quark t-channel, a $t\bar{t}$ and a background component, using the probability density functions described above. The mass is taken as the resulting value of the mean of the Gaussian core of

the Crystal Ball function fitting the single top contribution. All parameters of the single-top quark component are left floating in the fit; the difference between the peak position of the t-channel and the $t\bar{t}$ components is kept fixed to the value measured on simulation; all remaining parameters (including normalizations) are fixed to the values extracted from simulation.

The result of the fit to the full simulated sample is shown in Fig. 7 (left plot). The fitter takes the event weights into account, in order to obtain realistic errors on the fitted parameters.

The result of the fit to the full data sample is shown in Fig. 7 (right plot). The resulting value of the top quark mass is $m_t = 166.56 \pm 0.78\,\text{GeV}$ (statistical error only). By use of the mass calibration curve (Fig. 5) we determine the correction to be applied as $5.94 \pm 0.38\,\text{GeV}$.

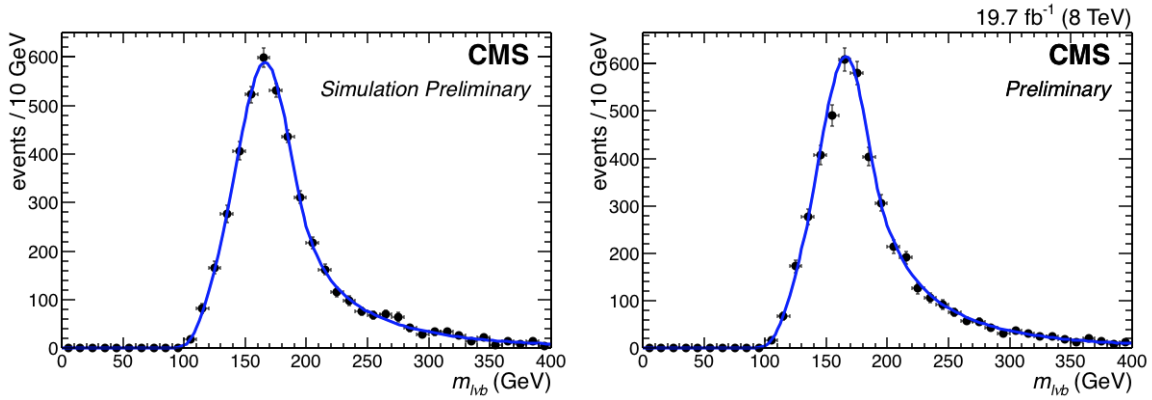

Figure 7: Result of the fit to the top invariant mass shape. Left: Monte Carlo; right: real data. The solid blue line represents the fitted PDF.

4.4 Cross checks

We assess the goodness of the fit and the fit stability using pseudo-experiments. We simulate ensembles of experiments starting from the signal and background templates and their normalization and vary them with Poissonian shifts. On each pseudo-experiment, we repeat the same fit described above and derive the top-quark mass and the signal yield. The resulting distributions of the top-quark mass and its error show that the fit does not have any significant bias, with the pull for the the top-quark mass distributed as expected, with no bias and errors correctly estimated.

The same check, repeated in the case where the central values of the two peaking distributions (single-top quark, t-channel, and other top-quark components) are left independent in the fit, gives opposite results, with very broad distributions of the central values, and large associated statistical errors. The corresponding pull distributions also do not match the expectations for an unbiased fit.

The mass measurement for the single top contribution is derived after having removed the single anti-top events. As a check, we repeated the analysis and measured the top-quark mass using only single anti-top events: we obtain a difference of $0.82 \pm 1.16\,\text{GeV}$ between the top-quark mass measured with single top and single anti-top events ($-0.6 \pm 1.5\,\text{GeV}$ expected from simulation).

5 Systematic uncertainties

Several sources of systematic uncertainties affect the measurement. While evaluating their contribution, we aimed at having a consistent error categorization in order to perform unambiguous combination of the results and we followed the general strategy adopted in [6].

In the following we describe the sources of uncertainties we identify as relevant for the measurement, as well as the procedure adopted to evaluate their impact.

5.1 Jet Energy Scale

Since we use jets with energies corrected on the basis of constant jet energy scale (JES) factors, we have to take into account the influence of the p_T - and η-dependent jet energy uncertainties. This is done by scaling the energies of all jets up and down according to their individual uncertainties, as determined by CMS in dedicated studies [22].

The uncertainties on the JES are grouped into different categories following the prescription defined in [23]. In order to estimate these uncertainties, for each of the categories above we re-determine the jet momenta, and all quantities which depend on them, by applying the jet corrections. We then repeat the fit on the simulated sample and take the shift with respect to the nominal fit as a measure of the uncertainty. For the 'Flavour correlation group', in order to refine the estimate, we apply, to each jet, the correction specific to its flavor, as inferred from the Monte Carlo truth information.

5.2 b-quark JES and Hadronization Modeling

This is the term which accounts for the b-flavour dependent uncertainties arising from the simulation of the parton-jet modeling and the accompanying JES uncertainty.

The total uncertainty can be decomposed into the sum of three separate contributions: a flavor-dependent JES term, the b-fragmentation uncertainty and the uncertainty from the B-hadron decays. The JES term is already included in the 'Flavour' term of the JES uncertainty reported above.

The b-fragmentation uncertainty was derived in the same fashion as for the top-quark mass measurement with semi-leptonic $t\bar{t}$ events [24]. The Bowler-Lund fragmentation function for B hadrons is retuned to agree with the x_B data measured by the ALEPH [25] and DELPHI [26] collaborations. A weight is attributed to each event, according to the x_B value, and the difference with respect to the nominal set-up is taken as the systematic uncertainty. We obtain an uncertainty on the top-quark mass of ± 0.02 GeV.

The systematic uncertainty from the semi-leptonic branching ratio of B hadrons is taken from the top-quark mass measurement with semi-leptonic $t\bar{t}$ events [24], in which the branching fractions were varied by 0.45% and $+0.77$% to give an envelope of the measurements from B^0/B^+ decays and their uncertainties.

5.3 Jet Energy Resolution

After correcting for the mismatch between the data and simulation for the energy resolution, the uncertainty is determined by varying the corrected jet-energy resolution (JER) using the η-dependent $\pm 1\sigma$ variations.

5.4 Lepton Energy Scale

The uncertainty is determined by varying the reconstructed lepton energies by $\pm 1\sigma$.

5.5 Unclustered Missing Transverse Energy

The uncertainty from particle-flow candidates not clustered within any jet is determined by varying the unclustered $E_{\mathrm{T}}^{\mathrm{miss}}$ by $\pm 10\%$.

5.6 Pile-up

This is the uncertainty coming from the modeling of the hadronic pile-up in the data. This is taken as the sum of the uncertainty due to the pileup variation (using pseudo-experiments in which the average number of pileup interactions was varied by $\pm 5\%$) and the pileup term extracted from the JES uncorrelated group (see above).

5.7 b-tagging Efficiencies

This is the uncertainty that results from using the p_{T}-dependent uncertainties on the b-tag and misidentification efficiencies to calculate a single systematic term.

5.8 Fit Calibration

We do not fix any parameters for the signal shape, hence we are not affected by any contributions from fixing parameters to the values determined on the simulation. We do however shift the measured mass on data by the shift measured on signal Monte Carlo events with respect to the input value to the simulation. The systematic uncertainty associated to this correction is evaluated by means of the calibration curve shown in Fig. 5, right. As far as the background component in the fit is concerned, its uncertainty is treated separately and described in the following.

5.9 Background Calculations

This is the uncertainty resulting from the use of simulated background in the mass determination. In this context, we treat both $\mathrm{t\bar{t}}$ and W+jets as backgrounds. One contribution to the systematic uncertainty is determined by varying the background normalizations by $\pm 1\sigma$ of their uncertainties. The overall effect on the mass is an uncertainty of ± 0.14 GeV. In addition, in the fit, we fix the PDF parameters of both the $\mathrm{t\bar{t}}$ and the W+jets components. We vary the fixed parameters within 1σ of their uncertainty.An additional contribution is listed under "Radiation and Matrix Element-Parton Shower Matching" owing to the fact that we take templates for the background components from the simulation, and uncertainties on the theoretical parameters used in input to the simulation may change the background shapes.

5.10 Generator Modeling

This contribution accounts for the fact that we use a signal MC sample produced with a 5-flavor scheme, that is by treating b-parton jets like light-quark jets. A comparison with a 4-flavour-scheme sample gives an estimate of the systematic uncertainty due to treating the b quarks like the light quarks. We evaluate this systematic uncertainty using single-top quark t-channel samples generated with the CompHEP generator [27]: these represent matched 4-flavour- and 5-flavour-scheme (2 to 3 and 2 to 2) LO samples, produced with exactly the same configurations.

5.11 Hadronization Modeling

This uncertainty is already covered by the JES uncertainty, and b-quark JES and hadronization uncertainties considered above. As a cross check, we compared the result obtained from a

POWHEG +HERWIG sample with that expected from the nominal POWHEG +PYTHIA simulation. A difference of 0.14 GeV is obtained.

5.12 Radiation and Matrix Element-Parton Shower Matching

This is the category which covers the QCD factorization and renormalization scales (Q^2) and initial- and final-state radiation uncertainties. We use dedicated MADGRAPH samples in which the Q^2-scales or matrix element-parton shower thresholds have been adjusted.

For the Q^2-scale, MADGRAPH samples with Q^2 scale shifted up or down by a factor of 4 are used. The uncertainty is determined by comparing the central result with the shifted ones. For the matrix element-parton shower matching thresholds, a factor of 2 up and down is used, with the systematic uncertainty evaluated in the same way as for the Q^2-uncertainty.

The signal dataset that we use is an unmatched sample, hence for the signal only the shift of the Q^2 scale is relevant.

5.13 Underlying Event

This term represents the uncertainty coming from the modeling of the underlying event (UE), the particles from the interaction that do not enter into the hard parton-parton interaction. It is evaluated by comparing the results from PYTHIA with alternative tunings [28]. The differences in the value of the fitted mass are within the statistical error determined by the size of the simulated samples. In fact the two opposite variations result in mass shifts with the same sign. For this reason, we estimate the uncertainty from this source as the maximum statistical uncertainty of the variations.uncertainty on the mass of ± 0.20 GeV.

5.14 Colour Reconnection

This uncertainty is evaluated by comparing two different UE tunes in which one has the nominal CR effects and the other has these turned off.

5.15 Parton Distribution Functions

We followed the PDF4LHC [29] prescriptions to calculate the uncertainty due to the choice of the parton distribution functions (PDF). We estimated the variation of the fitted top mass when using an alternative set of PDFs with respect to the nominal one, namely from the CT10, MSTW2008CP and NNPDF23 collections [30], [31], [32].

5.16 Summary of the Systematics Uncertainties

To summarize, the systematic uncertainties that affect the top-quark mass measurement, categorized according to the prescriptions, are reported in Table 1.

6 Results

The top-quark mass is measured in a sample enriched in single-top quark t-channel events, with a purity of 75%. The measured value is $m_t = 172.60 \pm 0.77\,(\text{stat})^{+0.97}_{-0.93}\,(\text{syst})$ GeV. This is in very good agreement with the current world average, based on measurements with $t\bar{t}$ events. Future improvements may include the addition of the electronic decay channel and the study of 13 TeV collision data: the signal cross section will be larger, however the $t\bar{t}$ background cross section will grow even more, requiring a re-optimization of the selection.

Table 1: Systematic uncertainties on the top-quark mass, in GeV.

Source	Subcategory	Uncertainty
	In-situ correlation group	$^{+0.20}_{-0.21}$
	Flavour correlation group	$^{+0.40}_{-0.40}$
	Inter-calibration group	$^{+0.00}_{-0.03}$
	Uncorrelated group	$^{+0.48}_{-0.40}$
	Pile-up p_T uncertainty	$^{+0.18}_{-0.10}$
Total JES		$^{+0.68}_{-0.61}$
b-quark JES and Hadronization Modeling		± 0.15
JER		< 0.05
Lepton energy scale		< 0.05
$E_{\mathrm{T}}^{\mathrm{miss}}$		± 0.15
Pile-up		± 0.10
b-tagging efficiency		± 0.10
Fit Calibration		± 0.38
	Background PDFs	± 0.10
	Background normalization	± 0.14
	Background Q^2 scale	± 0.18
	Background matching scale	± 0.30
Total Background Calculations		± 0.39
Generator modeling		± 0.10
Signal Q^2 scale		± 0.23
Underlying Event		± 0.20
Color Reconnection		< 0.05
PDF		< 0.05
Total		$^{+0.97}_{-0.93}$

References

[1] CDF and D0 Collaboration, "Combination of measurements of the top-quark pair production cross section from the Tevatron Collider", *Phys. Rev. D* **072001** (2014) 89.

[2] CMS Collaboration, "Measurement of the t-channel single-top-quark production cross section and of the $|V_{tb}|$ CKM matrix element in pp collisions at $\sqrt{s}$= 8 TeV", *JHEP* **06** (2014) 090, doi:10.1007/JHEP06(2014)090, arXiv:1403.7366.

[3] ATLAS Collaboration, "Measurement of the Inclusive and Fiducial Cross-Section of Single Top-Quark *t*-Channel Events in *pp* Collisions at $\sqrt{s}$ = 8 TeV",.

[4] N. Kidonakis, "Differential and total cross sections for top pair and single top production", arXiv:1205.3453.

[5] CMS Collaboration, "Top quark mass combinations using the 2010, 2011 and 2012 data",.

[6] CMS Collaboration, "Measurement of the top quark mass using proton-proton data at $\sqrt{s}$ = 7 and 8 TeV", arXiv:1509.04044.

[7] ATLAS Collaboration, "Measurement of the top quark mass in topologies enhanced with single top quarks produced in the t-channel at $\sqrt{s} = 8$ TeV using the ATLAS experiment", *ATLAS-CONF-2014-055*.

[8] CMS Collaboration, "The CMS experiment at the CERN LHC", *JINST* **3** (2008) S08004, doi:10.1088/1748-0221/3/08/S08004.

[9] S. Alioli et al., "A general framework for implementing NLO calculations in shower Monte Carlo programs: the POWHEG BOX", *JHEP* **06** (2010) 043, doi:10.1007/JHEP06(2010)043.

[10] T. Sjöstrand, S. Mrenna, and P. Skands, "PYTHIA 6.4 physics and manual", *JHEP* **05** (2006) 026, doi:10.1088/1126-6708/2006/05/026, arXiv:hep-ph/0603175.

[11] J. Alwell et al., "MadGraph 5: going beyond", *JHEP* **06** (2011) 128, doi:10.1007/JHEP06(2011)128.

[12] P. Nadolsky et al., "Implications of CTEQ global analysis for collider observables", *Phys. Rev. D* **78** (2008) 013004, doi:10.1103/PhysRevD.78.013004.

[13] D. J. Lange, "The EvtGen particle decay simulation package", *Nucl.Instrum.Meth.* **A462** (2001) 152–155.

[14] CMS Collaboration, "Particle–Flow Event Reconstruction in CMS and Performance for Jets, Taus, and $E_{\mathrm{T}}^{\mathrm{miss}}$", CMS Physics Analysis Summary CMS-PAS-PFT-09-001, 2009.

[15] CMS Collaboration, "Commissioning of the Particle-Flow Reconstruction in Minimum-Bias and Jet Events from pp Collisions at 7 TeV", CMS Physics Analysis Summary CMS-PAS-PFT-10-002, 2010.

[16] M. Cacciari, G. P. Salam, and G. Soyez, "The anti-k_t jet clustering algorithm", *JHEP* **04** (2008) 063, doi:10.1088/1126-6708/2008/04/063, arXiv:0802.1189.

[17] CMS Collaboration, "Determination of jet energy calibration and transverse momentum resolution in CMS", *JINST* **6** (2011) 11002, doi:10.1088/1748-0221/6/11/P11002.

[18] CMS Collaboration, "Identification of b-quark jets with the CMS experiment", *JINST* **8** (2013) 04013, doi:10.1088/1748-0221/8/04/P04013.

[19] CMS Collaboration, "Measurement of the t-channel single top quark production cross section in pp collisions at $\sqrt{s} = 7$ TeV", *JHEP* **12** (2012) 035, doi:10.1007/JHEP12(2012)035.

[20] T. Skwarnicki, "A study of the radiative cascade transitions between the Υ′ and Υ resonances",. DESY-F31-86-02.

[21] Belle Collaboration, "A detailed test of the CsI(Tl) calorimeter for BELLE with photon beams of energy between 20-MeV and 5.4-GeV", *Nucl.Instrum.Meth.* **A441** (2000) 401–426, doi:10.1016/S0168-9002(99)00992-4.

[22] "8 TeV Jet Energy Corrections and Uncertainties based on 19.8 fb^{-1} of data in CMS",. CMS Detector Performance Note CMS-DP-2013-033.

[23] CMS and ATLAS Collaboration, "Jet energy scale uncertainty correlations between ATLAS and CMS at 8 TeV",.

[24] CMS Collaboration, "Measurement of the top-quark mass in t t-bar events with lepton+jets final states in pp collisions at $\sqrt{s}$ = 8 TeV",. CMS-PAS-TOP-14-001.

[25] ALEPH Collaboration, "Study of the fragmentation of b quarks into B mesons at the Z peak", *Phys. Lett.* **B 512** (2001) 30–48, doi:10.1016/S0370-2693(01)00690-6.

[26] DELPHI Collaboration, "A study of the b-quark fragmentation function with the DELPHI detector at LEP I and an averaged distribution obtained at the Z Pole", *Eur. Phys. J.* **C 71** (2011) 1557, doi:10.1140/epjc/s10052-011-1557-x.

[27] E. Boos et al., "CompHEP - computer system for calculation of particle collisions at high energies ", *SINP MSU* **report 89-63/140** (1989).

[28] P. Skands, "Tuning Monte Carlo generators: The Perugia tunes", *Phys. Rev. D* **82** (2010) 074018, doi:10.1103/PhysRevD.82.074018.

[29] M. Botje et al., "The PDF4LHC Working Group Interim Recommendations", arXiv:1101.0538.

[30] P. M. Nadolsky et al., "Implications of CTEQ global analysis for collider observables", *Phys. Rev. D* **78** (2008) 013004.

[31] H.-L. Lai et al., "New parton distributions for collider physics", *Phys. Rev. D* **82** (2010) 074024.

[32] A. Martin et al., "Parton distributions for the LHC", *Eur.Phys. J. C* **63** (2009) 189285.